Heliyon 9 (2023) e18854

Contents lists available at ScienceDirect

Heliyon

journal homepage: www.cell.com/heliyon

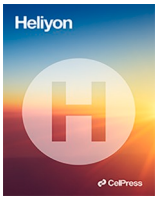

A posterior tibial slope angle over 12 degrees is critical to epiphyseal fracture of the proximal tibia: Three-dimensional finite element analysis

Hiroshi Watanabe [a,b,*], Kohei Murase [c], DongWook Kim [d], Takeo Matsumoto [d], Tokifumi Majima [b]

[a] Department of Orthopaedic Surgery, Nippon Medical School, Musashi Kosugi Hospital, Japan
[b] Department of Orthopaedic Surgery, Nippon Medical School, Japan
[c] Graduate School of Engineering Science, Osaka University, Japan
[d] Department of Mechanical and Aerospace Engineering, Faculty of Engineering, Nagoya University, Japan

ARTICLE INFO

Keywords:
Load-bearing
Shearing force
Athlete adolescent
Sports activity
Knee extensor mechanism

ABSTRACT

Introduction: The effects of the proximal tibial slope angle on the proximal tibial epiphysis remain unknown. To elucidate those effects, we investigated the strain distribution in proximal tibial epiphysis with different proximal tibial slope angles and proximal tibial epiphysis closure periods using finite element analysis.

Materials and methods: The finite element models of the proximal tibia were reconstructed from CT images and consisted of cancellous/cortical bone and epiphyseal plate. The variations in proximal tibial slope angle (range: 6–16°) and four closure variations in proximal tibial epiphysis (open, semi-open, semi-closed, and closed) were prepared. The loading force on the medial and lateral joint surface, and the tensile force by the patellar tendon were applied to the models, and the distal area of the tibia was fixed. The ratio of the equivalent strain in semi-open/semi-closed proximal tibial epiphysis to the strain in open proximal tibial epiphysis on different proximal tibial slope angles were calculated.

Results: The strain ratio between the semi-open/semi-closed and open proximal tibial epiphysis models indicated significant differences between 6 or 8° of proximal tibial slope angle and 12, 14, and 16° of proximal tibial slope angle models. In the increased proximal tibial slope angle model, a hoop-shaped strain in the closing proximal tibial epiphysis was found, and the maximum strain was found in the tibial tubercle.

Discussion: During epiphyseal closure, adolescents with an increased proximal tibial slope angle over 12° are significantly at risk for suffering from proximal tibial epiphyseal fractures compared with those under 10°.

1. Introduction

It is known that an increased proximal tibial slope angle (PTSA) is associated with the risk of sports-associated knee injuries such as

* Corresponding author. Department of Orthopaedic Surgery, Nippon Medical School, 1-383 Kosugi-machi, Nakahara-ku, Kawasaki, Kanagawa, 211-8533, Japan.
E-mail address: watanabehiroshi@nms.ac.jp (H. Watanabe).

https://doi.org/10.1016/j.heliyon.2023.e18854
Received 25 June 2023; Received in revised form 27 July 2023; Accepted 31 July 2023
Available online 2 August 2023

anterior cruciate ligament (ACL) injury [1–3]. The influence of PTSA in ACL injury has been investigated in a finite element study [4, 5]. Meanwhile, contrary to the large body of literature regarding the effects of PTSA on ACL injuries, the association between PTSA and the proximal tibial epiphysis (PTE) remains unclear. Since most epiphyseal injuries appear to resolve with conservative treatment, contrary to ACL injury, the exact incidence or evidence of PTE injury remains unknown. Recently, in our previous study, we reported the association of increased PTSA and Salter-Harris II proximal tibial fracture, and described how the source of the fracture force and how the resultant force of the anterior cruciate ligament and patellar tendon is interestingly in the opposite direction of the resultant force of the axial loading force and the anterior tibial translation force due to an increased PTSA [6] (Fig. 1). However, those analyses were limited in the two-dimensional sagittal plane using the vector diagram, and moreover, the precise strain distribution on PTE with the different PTSAs in three dimensions remains elusive. Because the epiphysis is a unique physical component only found until the growth period, it is difficult to investigate the research on epiphysis in clinical biomechanics using adolescent cadavers. Considering these ethical and clinical perspectives, a simulational study in silico would be suitable to study the strain distribution in PTE.

One of the characteristics of epiphysis is vulnerability due to its unique morphology. The Epiphysis is a developmental area for adolescents bone during growth stage, and moreover, it has multilayer structures. Among five zones (reserve, hypertrophic, degenerative, proliferative, and primary spongiosa zones), the proliferative zone has been revealed to be the most vulnerable to injury [7,8]. Therefore, until the complete closure of the epiphysis, epiphyseal fractures have been reported as one of the common sports-related injuries during adolescence [9]. During all epiphyseal fractures, the unique closure process of the proximal tibial epiphysis (PTE) from posterior to anterior direction in the end of the growth spurt period would also contribute the unique character of its fracture configuration [10].

Following our previous study on the association between increased PTSA and PTE fracture, the purpose of this study was set to determine how changes in PTSA affect equivalent strains in PTE at different periods of PTE closure during sports activities using finite element analysis and simulation.

2. Methods

To reach the objective, we used different models regarding different PTSAs (6, 8, 10, 12, 14, and 16°), and various closure situations of PTE (open, semi-open, semi-closed, and closed). The open epiphysis model simulated the open epiphyseal plate of children before the closing period. The semi-open and semi-closed models simulated the epiphyseal plates of adolescents whose epiphyseal plates are closing. The closed epiphysis model simulated the closed epiphyseal plate.

2.1. Sample collection

The computed tomography (CT) images of healthy teenage male subjects who reported no musculoskeletal disorder, pain, and previous knee surgery and who suffered a Salter-Harris II proximal tibial fracture were collected (Discovery CT750 HD, GE Healthcare, Milwaukee, USA). The proximal tibia of one healthy male and the proximal tibia of an injured male (contralateral side of the injured side) were delivered in the format of DICOM data, which consisted of slices of 1 mm pixels in three planes: axial, coronal, and sagittal directions.

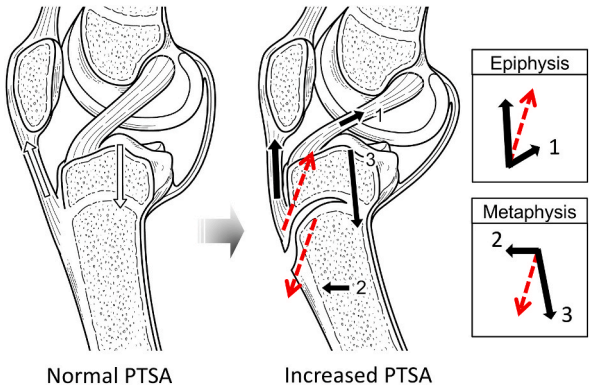

Fig. 1. Schematic diagram illustrating the injury mechanism of epiphyseal fractures of the proximal tibia. The images show a partially open physis of the proximal tibia. In a proximal tibia with an increased PTSA (right), increasing tension on the ACL (1) and anterior tibial translation (2) occur during jump or landing during sports activities with an axial loading force at the posterior proximal tibia (3). The resultant forces on the epiphysis and metaphysis change in contrast across the proximal tibial epiphysis. The forces shown as black arrows are summarized as resultant forces (red arrows) acting on the epiphysis and metaphysis, respectively. The resultant force produces shear movement at the anterior partially open physis of the proximal tibia. This shearing force is suggested to be the cause of epiphyseal fractures of the proximal tibia.

2.2. Reconstruction of CT scans

CT scans of proximal tibial bone were imported into the software MIMICS v10 (Materialize, Leuven, Belgium). Each pixel can be regenerated as part of the three-dimensional (3D) tibial bone structure in each plane. In this research, pixels were generated on the basis of the sagittal axis. Manually coloring each pixel formed a 3D block of bone slices. Cortical bone, cancellous bone, marrow and epiphyseal plates were generated.

2.3. Mesh model creation

2.3.1. Variation in epiphyseal closure

Four models with different epiphyseal closures were created: 1) open; 2) semi-open; 3) semi-closed; 4) closed epiphysis model. In the open epiphysis model, no boundary was created between the cortical and cancellous regions. For the semi-open epiphysis model, the posterior region of the epiphysis was divided into cortical and cancellous. For the semi-closed epiphysis model, the posterior and intermediate regions of the epiphysis were divided into cortical and cancellous regions. For the closed epiphysis model, all epiphyseal plate regions were divided into cortical and cancellous areas (Fig. 2a–d).

2.3.2. Mesh conditions

The 3D finite elements were created as a second order tetrahedral mesh (Fig. 3). The number of elements was approximately 9500. All material properties of the model parts (cortical, cancellous bones and epiphyseal plate) were determined from literature, and defined as isotropic elastic solids [11] (Table 1). To optimize the number of elements and determine the correctness, the mesh convergence test was carried out at node location #12 (Fig. 5).

2.3.3. Mesh-morphing techniques for various PTSA model creation

To produce proximal tibial models with different PTSAs, whole cortical and cancellous lesions were rotated on the midpoint of the medial tibial plateau at PTSAs of 6, 8, 10, 12, 14, and 16°. The evidence of PTSA variations is our previous study reporting that the mean PTSA of adolescents suffering Salter-Harris II proximal tibial fracture is between 13.6° and 16.8°, and the PTSA of healthy knee is around 9.6° [6].

Epiphyseal plates and bottom components of the proximal tibia (components below the epiphyseal plate) of rotated components were eliminated through Boolean transform. The refinement and smoothing of the 3D model of cortical, cancellous, and marrow bones were performed on the proprietary software 3-matic and Meshmixer (Materialize IV, Belgium).

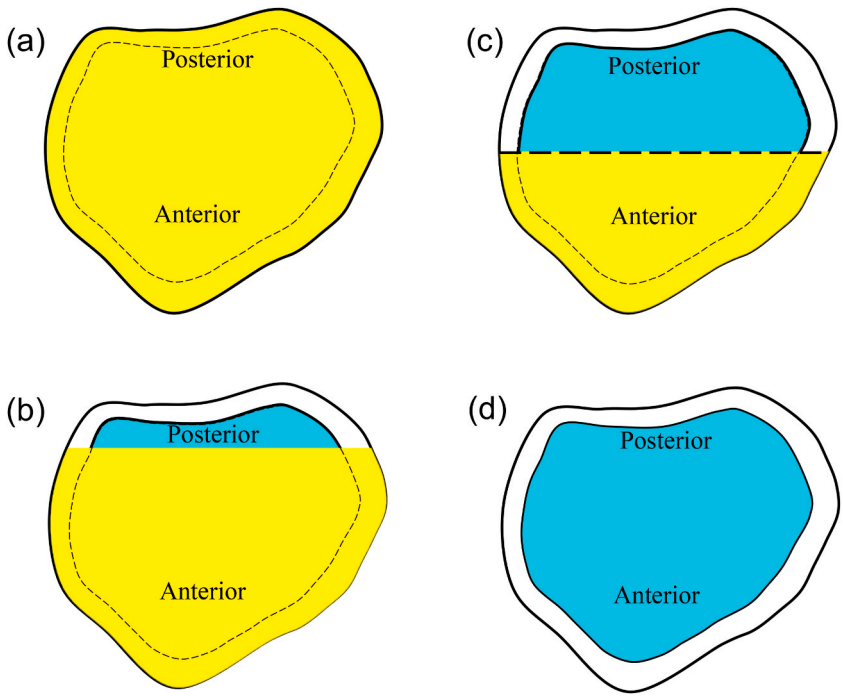

Fig. 2. Four models with different epiphyseal closures were created: a) open; b) semi-open; c) semi-closed; d) closed epiphysis model. The material color is as shown in Table 1.

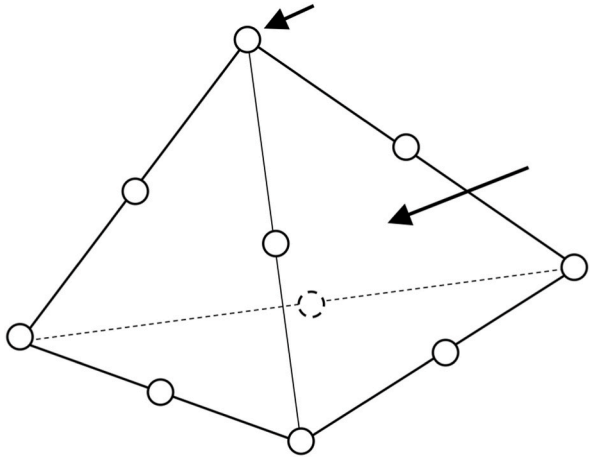

Fig. 3. The tetrahedron indicates the second order tetrahedral element (long arrow), and the white open circles on the apexes and the edges indicate the nodal points (short arrow).

Table 1
Material properties of the finite element model parts.

Material	Young's modulus [MPa]	Poisson's ratio
Cortical bone	4800	0.24
Cancellous bone	1000	0.31
Open epiphyseal plate	215	0.4

2.4. Loading conditions

To perform finite element analysis, the loading conditions were defined, according to the previous reports [12,13]. The force of patellar tendon was applied as tensile force and body weight were applied as loading forces both in a vertical direction (Fig. 4), as the tibial bone model was assumed to be in the jumping or landing phase. The following conditions were applied in Hyperworks software (Altair Engineering Inc., United States). Compressive force was applied to the medial and lateral tibial plateau. Tensile force was applied to the tibial attachment of the patellar tendon. The force applied regions were denoted by yellow nodal points, and the bottom of the proximal tibia was fixed (Fig. 4).

2.5. Finite element analysis (FEA)

The tibial model with loading conditions was exported as an Abaqus file for finite element analysis. The Abaqus file (.inp file) was exported to the open software Calculix for simulation (Convergent Mechanical, United States). The calculated Abaqus file was converted to a. vtk file for visualization in the open software Paraview (Kitware Inc., United States). For postdata processing, the nodal location along the side layer of the epiphyseal plate was set to quantify the equivalent strain distribution in the epiphyseal plate (Fig. 5).

2.6. Quantification of equivalent strain

Equivalent strain at the midpoint of the proximal tibial epiphyseal plate was calculated with
The following equation.

$$\varepsilon_{eq} = \frac{2}{3}\sqrt{\frac{3}{2}\left(e_{xx}^2 + e_{yy}^2 + e_{zz}^2\right) + \frac{3}{4}\left(\gamma_{xy}^2 + \gamma_{yz}^2 + \gamma_{zx}^2\right)}$$

Deviatoric strains e are defined as:

$$e_{xx} = \frac{2}{3}\varepsilon_{xx} - \frac{1}{3}\varepsilon_{yy} - \frac{1}{3}\varepsilon_{zz}$$

$$e_{yy} = -\frac{1}{3}\varepsilon_{xx} + \frac{2}{3}\varepsilon_{yy} - \frac{1}{3}\varepsilon_{zz}$$

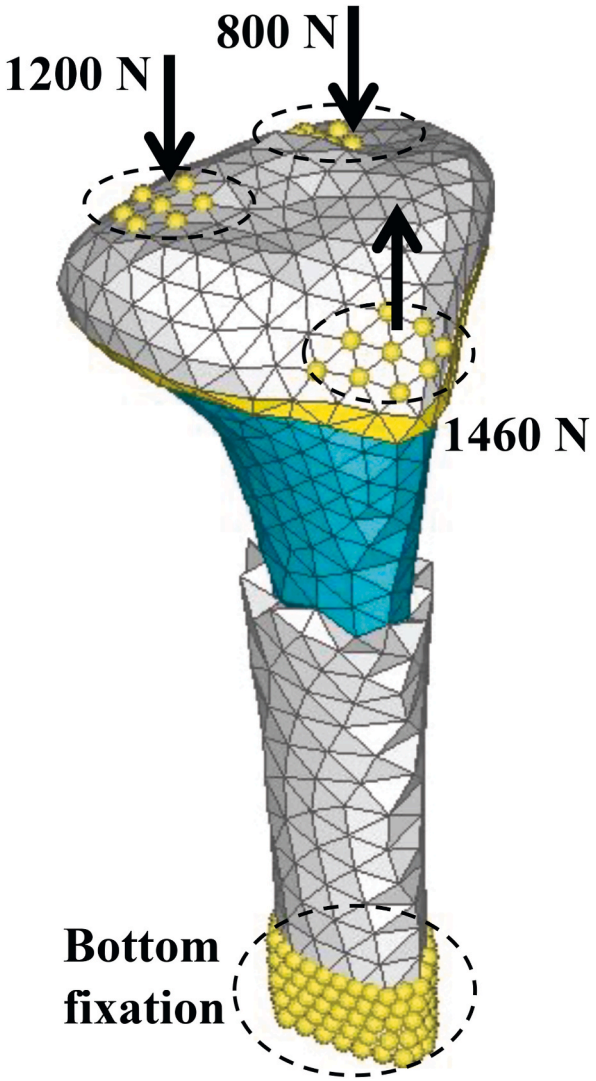

Fig. 4. The force applied regions were denoted by yellow nodal points, and the 180 mm distal area of the joint surface was fixed. Regarding each material, the cortical bone is white, the cancellous bone is blue, and the open epiphyseal plate is yellow.

$$e_{zz} = -\frac{1}{3}\varepsilon_{xx} - \frac{1}{3}\varepsilon_{yy} + \frac{2}{3}\varepsilon_{zz}$$

The engineering strains γ are defined as:

$$\gamma_{ij} = 2 \times \varepsilon_{ij}$$

Strain at different coordinates and axis were found from nodal point taken from the midpoint of the proximal tibial epiphyseal plate. With the equations above, the equivalent strain visualized in Paraview was quantified.

2.7. Statistical analyses

Statistical analysis was performed using SPSS software (version 22.0, IBM Corp., Armonk, NY, USA). The Kruskal-Wallis test with post-hoc comparisons (Bonferroni correction) was used to assess the multiple comparisons, due to the small number of each group (N = 7). Data were expressed as mean (SD; standard deviation). The level of significance was set at $P < 0.05$.

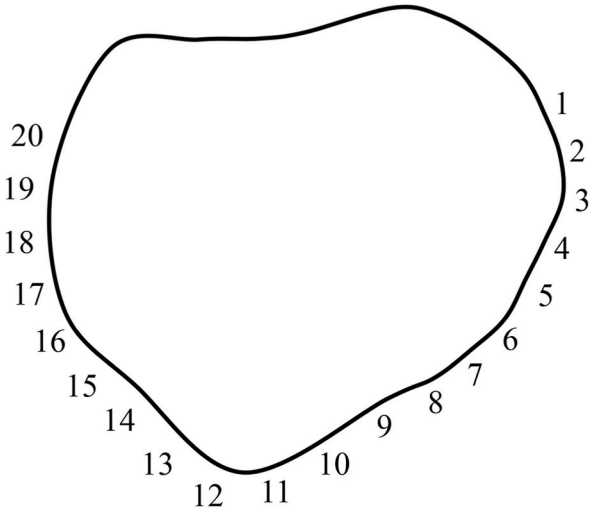

Fig. 5. The nodal location along the side layer of the epiphyseal plate was set to quantify the equivalent strain distribution in the epiphyseal plate (#1–20).

3. Results

3.1. Equivalent strain distribution with various epiphyseal closures

Equivalent strain was observed in this research using Paraview. The equivalent strain distribution was mainly increased at the anterior tip around the tibial tubercle of the epiphyseal plate, in the open, semi-open, and semi-closed models, and the equivalent strain of four different epiphyseal closure models at each nodal location is shown (Figs. 6–8).

3.2. Equivalent strain ratio

To analyze the tendency observed in Figs. 6–8, we calculated the equivalent strain ratio between the semi-open/semi-closed and open epiphysis models in the node of the tibial tubercle (#10–13) with the following equation (Table 2). We defined the equivalent strain ratio to evaluate the risk of proximal tibial epiphyseal fractures.

Strain ratio at each node location $\varepsilon_{\#x}$ was defined as:

$$\text{Strain ratio at node location } \#x\ (\varepsilon_{\#x}) = \frac{\text{Equivalent strain at } \#x}{\text{Equivalent strain at } \#x \text{ in open epiphysis model}}$$

Equivalent strain ratio (ε) of each model was defined as:

$$\text{Equivalent strain ratio } (\varepsilon) = \frac{1}{4}(\varepsilon_{\#10} + \varepsilon_{\#11} + \varepsilon_{\#12} + \varepsilon_{\#13})$$

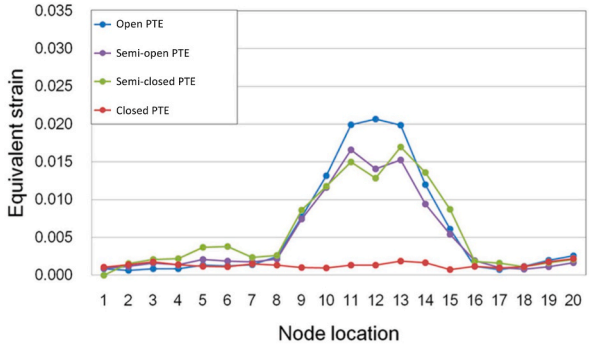

Fig. 6. The equivalent strain of four different epiphyseal closure models at each nodal location is shown at PTSA of 6° (Fig. 5).

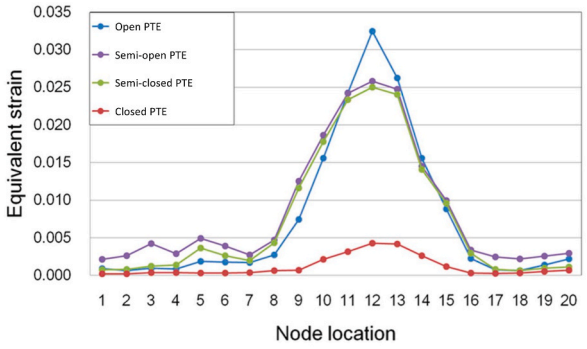

Fig. 7. The equivalent strain of four different epiphyseal closure models at each nodal location is shown at PTSA of 10° (Fig. 6).

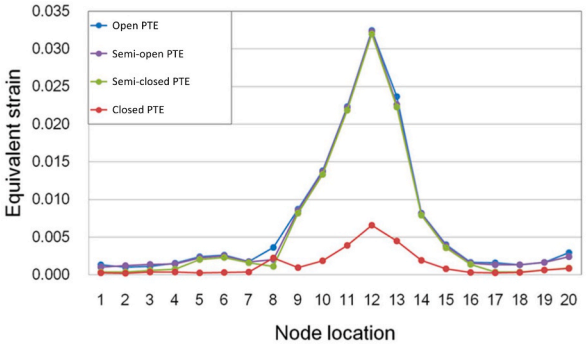

Fig. 8. The equivalent strain of four different epiphyseal closure models at each nodal location is shown at PTSA of 16° (Fig. 7).

Table 2
The equivalent strain ratio (ε) at each PTSA, on the models with different epiphyseal closures.

PTSA (deg.)	*ε (semi-open)*	*ε (semi-closed)*	*ε (closed)*
6	0.792 ± 0.0745	0.782 ± 0.105	0.0867 ± 0.0141
8	0.950 ± 0.144	0.792 ± 0.116	0.135 ± 0.00998
10	0.983 ± 0.143	0.947 ± 0.132	0.145 ± 0.0133
12	0.976 ± 0.0256	0.960 ± 0.0249	0.199 ± 0.0340
14	0.966 ± 0.0366	0.945 ± 0.0369	0.140 ± 0.0229
16	0.982 ± 0.0167	0.967 ± 0.0169	0.187 ± 0.0301

*All values are shown as mean ± standard deviation.

3.3. Statistical results

The significant difference between PTSA >12° and PTSA <8° group was more evident in the equivalent strain ratio between the semi-closed and open epiphysis models than the equivalent strain ratio between the semi-open and open epiphysis models (Figs. 9 and 10) ($p < 0.05$). In the increased PTSA model, a hoop-shaped strain in the closing PTE was found, and the maximum strain was confirmed in the tibial tubercle region of the closing PTE (Fig. 11).

4. Discussion

To investigate the mechanism of epiphyseal fractures in adolescent athletes, computational modeling has the advantage of simulating the role of PTSA on PTE. In the current study, we computed the effects of changes in PTSA on PTE in the 3D finite element method (FEM). The critical effects of increased PTSA on the proximal tibial epiphysis during jumping or landing, and the precise strain distribution of the proximal tibial epiphysis were investigated using FEM. In the computed results of the current study, the increased PTSA could affect the strain distribution, mainly at the anterior tip of the tibial tubercle, among the semi-open and semi-closed PTE (Figs. 6–8, 11). The equivalent strain ratio between the semi-open/semi-closed and open epiphysis models shows that the shearing strain in PTE is significantly different between 6 or 8° of PTSA and 12, 14, and 16° of PTSA (Figs. 9 and 10). Because the epiphysis is not flat, but 3-dimensionally complicated in shape, therefore, we calculated the equivalent strain, considering the effects of shearing force. In addition, the loading force is not even between medial and lateral side, therefore we did not calculate the principal stress in the

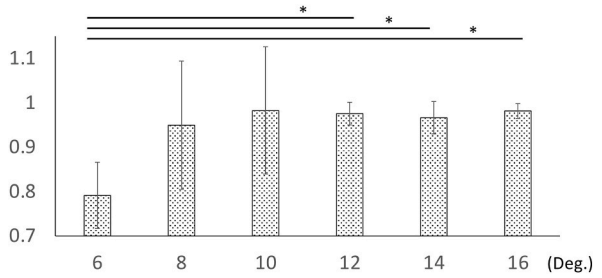

Fig. 9. The equivalent strain ratio between the semi-open and open epiphysis model in the node of the tibial tubercle (#10–13). The asterisk denotes a statistically significant difference during models of different PTSA at the 0.05 level, as derived from the Kruskal-Wallis test with post-hoc comparisons (Bonferroni correction).

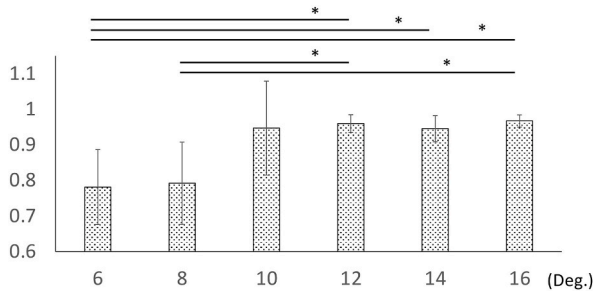

Fig. 10. The equivalent strain ratio between the semi-closed and open epiphysis model in the node of the tibial tubercle (#10–13). The asterisk denotes a statistically significant difference during models of different PTSA at the 0.05 level, as derived from the Kruskal-Wallis test with post-hoc comparisons (Bonferroni correction).

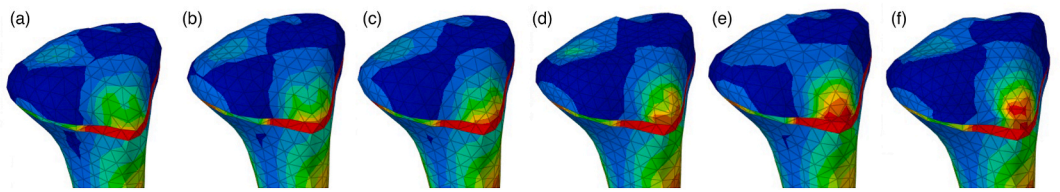

Fig. 11. Diagrams to show the models with different PTSA of 6 (a), 8 (b), 10 (c), 12 (d) 14 (e), and 16 (f) degrees. A hoop-shaped strain in the closing PTE was found, and the maximum strain was confirmed in the tibial tubercle region of the closing PTE.

current study. Our previous study was reporting that the mean PTSA of adolescents suffering Salter-Harris II proximal tibial fracture was over 13.6°, and meanwhile, the PTSA of healthy adolescents was around 9.6° [6]. Moreover, in the current study, the results showed the significant difference between PTSA >12° and PTSA <8° groups. Taken together, the threshold of epiphyseal fracture would be from 10 to 12° of PTSA, and a PTSA over 12° is considered critical for epiphyseal fractures of the proximal tibia. These results in the current study support our proposed injury mechanism of epiphyseal fractures of the proximal tibia, which described the shearing force at the anterior proximal tibia as the fracture force of flexion-type SH II fractures of the proximal tibia [6] (Fig. 1). In addition, our results of the normal PTSA model indicate that PTE has little strain on the anterior tip of the PTE during sports activities in healthy adolescents with normal PTSA.

Most of the previous case reports have only suggested quadriceps muscle contraction in jumping or landing as the primary cause, since the mechanisms of epiphyseal fractures of the proximal tibia have been poorly understood [14,15]. In the current study, we added the FEM data to our mechanism configuration of proximal tibia epiphyseal fractures, making it more suitable.

In addition to the reports about associations between ACL and PTSA, studies regarding associations between PTSA and knee stability, such as the effect of PTSA on knee biomechanics during functional activity [16,17], knee stability after PCL injury [18], and the geometry of the tibial plateau and its influence on the biomechanics of the tibiofemoral joint [19], have been reported recently. Considering these previous reports, PTSA contributes greatly to knee kinematics.

In our results, the strain concentrates at the interface between the open epiphyseal plate and proximal tibial cortical bone, and therefore a 'hoop-shaped' high strain distribution was observed on the surface of the PTE. It was considered that the epiphyseal plate of the increased PTSA model applied not only the tensile force from the patellar tendon but also a larger loading moment that was generated by the PTSA angle compared with the normal knee.

When interpreting the results of this study, several limitations should be taken into account. First, the variety of anatomical and physiological configurations was not considered in the current study. Second, we should investigate more dynamic factors in the mechanism of PTE injury in the future. Third, because of the wide variety of properties of proximal tibia which consists of cortical bone, cancellous bone, and the epiphyseal plate, we calculated the strain, without using the stress for FEA in the current study. Fourth, we focused on the stress variation's tendency on whole entire proximal tibial epiphysis, therefore, we used the coarser mesh patterns with second order tetra element where the lengths of the average elements were 3–5 mm.

5. Conclusions

During epiphyseal closure, adolescents with an increased PTSA over 12° are significantly at risk for suffering proximal tibial epiphyseal fractures compared with those with a PTSA under 10°.

Ethics statement

This study was conducted in accordance with the ethical standards of the Declaration of Helsinki, and the institutional ethics review board of our hospital approved the study protocol (approval number #663-4-37).

Author contribution statement

Hiroshi Watanabe: Conceived and designed the experiments; Performed the experiments; Analyzed and interpreted the data; Contributed reagents, materials, analysis tools or data; Wrote The paper. Kohei Murase: Conceived and designed the experiments; Performed the experiments; Analyzed and interpreted the data; Contributed reagents, materials, analysis tools or data. DongWook Kim: Performed the experiments; Analyzed and interpreted the data. Takeo Matsumoto; Tokifumi Majima: Conceived and designed the experiments.

Data availability statement

Data will be made available on request.

Additional information

No additional information is available for this paper.

Declaration of competing interest

The authors declare that they have no known competing financial interests or personal relationships that could have appeared to influence the work reported in this paper.

Acknowledgements

This work was supported by Japan Society for the Promotion of Science.(JSPS) Grants-in-Aid for Scientific Research (Grant Number JP 21K16695).

References

[1] M.L. Brandon, P.T. Haynes, J.R. Bonamo, M.I. Flynn, G.R. Barrett, M.F. Sherman, The association between posterior-inferior tibial slope and anterior cruciate ligament insufficiency, Arthroscopy 22 (2006) 894–899.
[2] S.T. Hendrix, A.M. Barrett, B. Chrea, W.H. Replogle, J.M. Hydrick, G.R. Barrett, Relationship between posterior-inferior tibial slope and bilateral noncontact ACL injury, Orthopedics 40 (2017) e136–e140.
[3] A. Waiwaiole, A. Gurbani, K. Motamedi, L. Seeger, M.S. Sim, P. Nwajuaku, S.L. Hame, Relationship of ACL injury and posterior tibial slope with patient age, sex, and race, Orthop J Sports Med 4 (2016), 2325967116672852.
[4] I. Kostogiannis, P. Swärd, P. Neuman, T. Fridén, H. Roos, The influence of posterior-inferior tibial slope in ACL injury, Knee Surg. Sports Traumatol. Arthrosc. 19 (2011) 592–597.
[5] H. Marouane, A. Shirazi-Adl, M. Adouni, J. Hashemi, Steeper posterior tibial slope markedly increases ACL force in both active gait and passive knee joint under compression, J. Biomech. 47 (2014) 1353–1359.
[6] H. Watanabe, T. Majima, K. Takahashi, N. Iizawa, Y. Oshima, S. Takai, Posterior tibial slope angle is associated with flexion-type Salter-Harris II and Watson-Jones type IV fractures of the proximal tibia, Knee Surg. Sports Traumatol. Arthrosc. 27 (2019) 2994–3000.
[7] T.S. Fujii T, Y. Arai, W. Kim, D. Amiel, Y. Hirasawa, Microstructural properties of the distal growth plate of the rabbit radius and ulna: biomechanical, biochemical, and morphological studies, J. Orthop. Res. 18 (2000) 87–93.
[8] F. Burdan, J. Szumiło, A. Korobowicz, R. Farooquee, S. Patel, A. Patel, A. Dave, M. Szumiło, M. Solecki, R. Klepacz, J. Dudka, Morphology and physiology of the epiphyseal growth plate, Folia Histochem. Cytobiol. 47 (2009) 5–16.
[9] D. Caine, J. DiFiori, N. Maffulli, Physeal injuries in children's and youth sports: reasons for concern? Br. J. Sports Med. 40 (2006) 749–760.
[10] V.M. Dvonch, W.H. Bunch, Pattern of closure of the proximal femoral and tibial epiphyses in man, J. Pediatr. Orthop. 3 (1983) 498–501.
[11] S.M. Nazemi, M. Amini, S.A. Kontulainen, J.S. Milner, D.W. Holdsworth, B.A. Masri, D.R. Wilson, J.D. Johnston, Prediction of local proximal tibial subchondral bone structural stiffness using subject-specific finite element modeling: effect of selected density-modulus relationship, Clin. Biomech. 30 (2015) 703–712.

[12] Q. Shao, T.D. MacLeod, K. Manal, T.S. Buchanan, Estimation of ligament loading and anterior tibial translation in healthy and ACL-deficient knees during gait and the influence of increasing tibial slope using EMG-driven approach, Ann. Biomed. Eng. 39 (2011 Jan) 110–121.
[13] L. Yin, D. Sun, Q.C. Mei, Y.D. Gu, J.S. Baker, N. Feng, The kinematics and kinetics analysis of the lower extremity in the landing phase of a stop-jump task, Open Biomed. Eng. J. (2015 Mar 31) 103–107.
[14] Y.N. Takai S, Y. Kubo, M. Suzuki, Y. Hirasawa, Bilateral epiphyseal fractures of the proximal tibia within a six-month interval- A case report, J. Orthop. Trauma 14 (2000) 585–588.
[15] S. Vyas, E. Ebramzadeh, C. Behrend, M. Silva, L.E. Zionts, Flexion-type fractures of the proximal tibial physis: a report of five cases and review of the literature, J. Pediatr. Orthop. B 19 (2010) 492–496.
[16] J.R. Giffin, T.M. Vogrin, T. Zantop, S.L. Woo, C.D. Harner, Effects of increasing tibial slope on the biomechanics of the knee, Am. J. Sports Med. 32 (2004) 376–382.
[17] K.B. Shelburne, H.J. Kim, W.I. Sterett, M.G. Pandy, Effect of posterior tibial slope on knee biomechanics during functional activity, J. Orthop. Res. 29 (2011) 223–231.
[18] C. Gwinner, A. Weiler, M. Roider, F.M. Schaefer, T.M. Jung, Tibial slope strongly influences knee stability after posterior cruciate ligament reconstruction: a prospective 5- to 15-year follow-up, Am. J. Sports Med. 45 (2017) 355–361.
[19] J. Hashemi, N. Chandrashekar, B. Gill, B.D. Beynnon, J.R. Slauterbeck, R.C. Schutt Jr., H. Mansouri, E. Dabezies, The geometry of the tibial plateau and its influence on the biomechanics of the tibiofemoral joint, J Bone Joint Surg Am 90 (2008) 2724–2734.